J. Fluid Mech. (1975), *vol.* 70, *part* 4, *pp.* 733–752
Printed in Great Britain

The laminar flow of dilute polymer solutions through porous media

By DAVID F. JAMES AND D. R. McLAREN
Department of Mechanical Engineering, University of Toronto, Canada

(Received 8 May 1974 and in revised form 12 December 1974)

Measurements of the pressure drop and flow rate were obtained for dilute solutions of polyethylene oxide flowing through beds of packed beads. When the velocity was sufficiently high, the pressure drop was above that for a Newtonian fluid of equal viscosity, often considerably above, and this viscoelastic effect was explored by varying the concentration and molecular weight of the polymer, by testing solutions over a wide range of flow rates, and by using several bead sizes. The non-Newtonian behaviour was most pronounced at moderate flow rates; at the highest velocities, the data were pseudo-Newtonian in character, i.e. the pressure drop still exceeded that for a Newtonian fluid, but was linearly related to the velocity. For some solutions, the large deviation from Newtonian values occurred over such a short range of flow rates that there was an interval in which the pressure drop *decreased* with velocity. It was not possible, therefore, to obtain steady-state measurements in this regime and a gap appears in the data curve of pressure *vs.* velocity.

The pressure drop was monitored in steps along the test section, so that it was possible to detect molecular degradation of the solutions as they flowed through the porous media. In general, degradation was not extensive and the solutions became stably degraded by the midpoint of the test section. Degradation increased with velocity and, quite surprisingly, became more severe as the bead size increased.

A visual examination of the flow field revealed that the streamline pattern for the polymer solutions was the same as that for water. The large non-Newtonian effects were therefore due to changes in the stress field, and in an effort to understand these effects, an analysis was carried out which examined how the stresses generated by each component of the deformation, i.e. by shear and pure strain, influence the pressure drop. This analysis, combined with a study of onset data, indicates that onset and the sudden large departures from Newtonian values are probably due to an interaction between extensional and shearing deformation, and that the reduced viscoelastic effect of higher flow rates may be due to the dominance of extensional stresses.

1. Introduction

Part of the current interest in dilute polymer solutions has been generated by the use of polymers to improve water-flooding in secondary oil recovery. In this process, water is injected underneath an oil reservoir to sweep the residual oil

from the porous formation upwards to the producing well. The greater the flow resistance of the water relative to the oil, the more efficient is the displacement process, and one means of increasing the viscosity of the water is to use soluble polymer additives. A good survey of field and laboratory studies of this method is included in a recent review article by Savins (1969) on non-Newtonian flow in porous media.

A number of prior investigations have sought to understand the improved oil recovery by examining the properties of solutions of high-weight polymers and their effect on the flow resistance. The majority of these studies used concentrated polymer solutions and related the higher pressure drops to the increase in viscosity. For example, Christopher & Middleman (1965) used carboxymethyl cellulose and polyisobutylene at concentrations of 1–6 % and correlated their data for flow through packed beads using the parameters of the power-law model of viscosity. For less concentrated solutions, the larger pressure drops can no longer be attributed solely to viscous effects because the increase may be an order of magnitude larger than the increase in viscosity. Consequently, elastic effects must also be taken into account, and changes in the flow are expected when the relaxation time of the elastic liquid is comparable to the characteristic time of the flow. This concept is supported by the experimental evidence of Sadowski (1965) and Marshall & Metzner (1967) for concentrated solutions. Dauben & Menzie (1967) investigated non-Newtonian effects in porous media with polyethylene oxide solutions, ranging from dilute to moderately concentrated, and they too found pressure losses which were much higher than those predicted using Darcy's law and the measured solution viscosity. However, they did not explain this anomaly in terms of viscoelastic properties, but related their data to the pore size and viscous power-law parameters. It appears that only Jones & Maddock (1969) have worked with strictly dilute solutions, viz., at concentrations sufficiently low that hydrodynamic interaction between macromolecules is negligible. They used four concentrations of polyacrylamide and one of sodium carboxymethyl cellulose, and were primarily interested in the onset of viscoelastic effects. In particular, they examined the conditions under which the pressure–flow data of the solutions departed from the solvent data, and compared these conditions with those for the onset of drag reduction in turbulent pipe flow.

The purpose of the present programme was to explore viscoelastic effects in porous media with very dilute solutions. The range of variables in Jones & Maddock's experiments produced only slight deviations from Newtonian behaviour, and it was thought that much larger viscoelastic effects were possible under different conditions. More pronounced viscoelasticity, it was reasoned, would provide more knowledge about the rheology of dilute solutions and might lead to a better understanding of the mechanism by which polymer additives reduce drag in turbulent wall flows. Previous work with dilute solutions and submerged cylinders (James & Acosta 1970) had shown that viscoelastic effects are large and are related to molecular parameters; in order to fully explore non-Newtonian behaviour for flow through packed beads, the present experiment was designed to allow a substantial variation of the flow parameters, including the flow rate, bead size, polymer concentration and molecular weight.

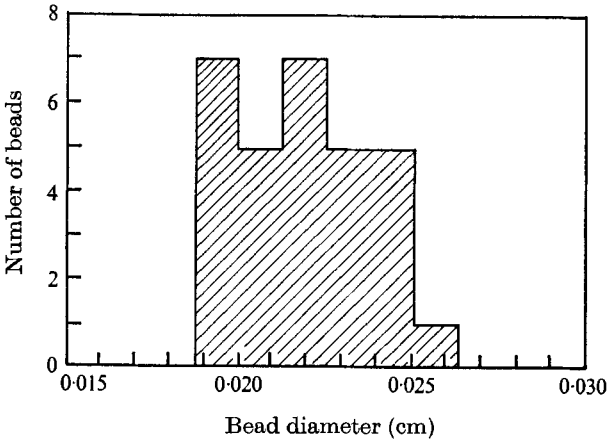

FIGURE 1. Histogram for a sample of 30 glass beads. The average diameter was determined from this histogram to be 0·022 cm.

2. The experimental method

The experiment essentially consisted of driving aqueous solutions of polyethylene oxide through columns of packed glass beads, and measuring the pressure drop and flow rate. The beads were a commercial product† normally used for reflecting surfaces and were sorted with U.S. Standard sieves to produce three sizes with narrow distributions. For each size, a sample of the population was examined under a microscope to measure the distribution of diameters and consequently to determine the average. The mean diameters determined by this technique were 0·011, 0·022 and 0·045 cm, and the distribution for a typical sample is shown in figure 1. The microscopic examination also revealed that about 86 % of the beads were true spheres, while the remainder were generally double or triple beads.

The beads were packed in Plexiglas tubes having a series of pressure taps, as illustrated in figure 2. Three such test cells were made in order to house beads of each of the three sizes, and the void fractions were measured to be 0·372, 0·377 and 0·368, in order of increasing bead size. The five pressure taps were installed to monitor the pressure drop along the length of the test section and thus to check the constancy of fluid and matrix properties. Pressure differences between adjacent taps were measured by a calibrated diaphragm-type transducer. The experimental fluids were driven through the test sections by an elevated, and sometimes pressurized, constant-head tank, and the discharge at the exit was collected to determine the flow rate. In order to validate the experimental technique, the first fluid tested was Newtonian, namely plain water. The results are plotted in figure 3 along with the modified Ergun equation, which represents an average of the considerable data of previous investigations for Newtonian fluids (Bird, Stewart & Lightfoot 1964). For this graph and others that follow, the

† From Flexolite of Canada Ltd.

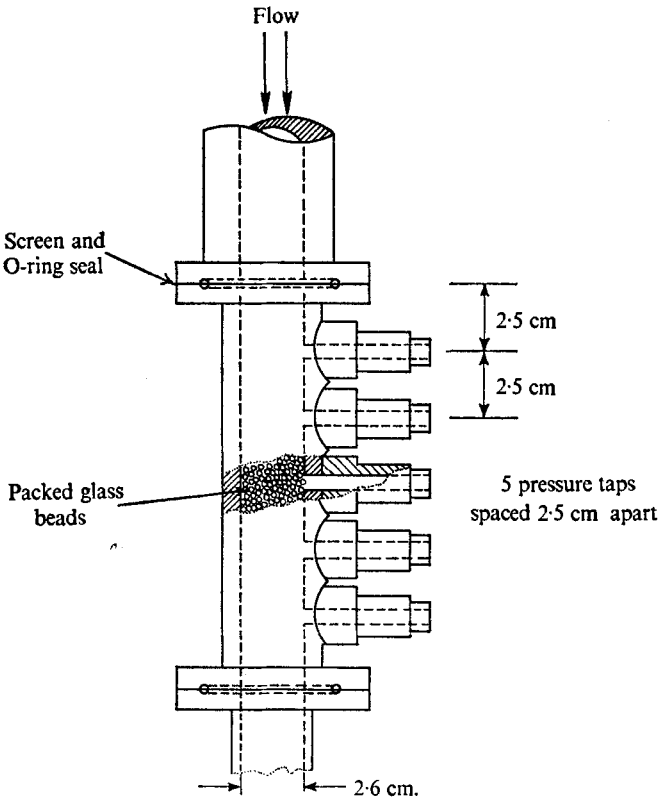

FIGURE 2. Test cell, packed with glass beads. Screens were placed at the entrance and exit of the cell and over the ports of the pressure taps.

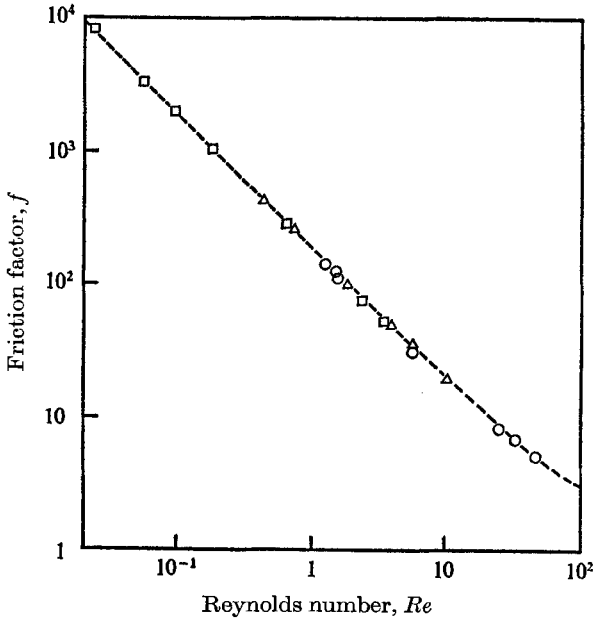

FIGURE 3. Friction-factor data for water; f and Re are the Ergun co-ordinates, defined in the text. ---, modified Ergun equation $f = 180/Re + 1{\cdot}75$, the curve fitted through previous results for Newtonian fluids (Bird *et al.* 1964). Bead diameter (mm): ○, 0·45; △, 0·22; □, 0·11.

Polyox grade	Polymer properties $[\eta]$	$\bar{M}_w$	K	Concentration c (p.p.m. by weight)	Kinematic viscosity at 25 °C ν (cS)
WSR-205	4·7	$9{\cdot}4\times10^5$	0·47	30	0·904
				60	0·918
				120	0·942
				240	0·998
				480	1·11
WSR-301	15	$4{\cdot}2\times10^6$	0·40	10	0·908
				20	0·919
				40	0·944
				80	1·00
				160	1·13
FRA	29	$9{\cdot}7\times10^6$	0·0	6	0·905
				12	0·918
				24	0·956
				48	1·03
				96	1·13

TABLE 1. Description of the polymer solutions tested in the porous media

pressure and flow-rate measurements are presented in terms of the Ergun (1952) co-ordinates

$$f = \rho\Delta p D\epsilon^3/G^2L(1-\epsilon), \quad Re = DG/\mu(1-\epsilon),$$

where Δp is the pressure drop (corrected for the elevation difference between pressure taps) over a length L, D is the bead diameter, ϵ the void fraction, G the mass flow rate per unit area, μ the fluid viscosity, and ρ the density. The good agreement of the present data with the modified Ergun equation in figure 3 is reassuring evidence of the reliability of our experimental system.

Dilute aqueous solutions of polyethylene oxide were then tested in the flow apparatus. This particular polymer was selected because it produced highly elastic solutions and because the relationship between its intrinsic viscosity $[\eta]$ and weight-average molecular weight M_w is known from Shin's (1965) correlation: $[\eta] = 1{\cdot}03\times10^{-4}M_w^{0{\cdot}78}$. Consequently the molecular weight of a sample was determined by finding $[\eta]$ from viscometric measurements, which were made with Cannon–Fenske bulb viscometers. Three grades of commercially available Polyox† where chosen, and for each grade various concentrations were tested to provide a range of viscoelastic behaviour. All concentrations were easily in the dilute regime since the product $[\eta]c$ was 0·3 at most, where c is the concentration. The details of the polymer solutions are given in table 1.

The polymer solutions listed in this table were too dilute to determine their intrinsic viscosity, and thus additional solutions of higher concentration were prepared for each grade. The viscometric data for one of the grades, WSR-301, are presented in figure 4 as an example. This plot shows the expected linear

† Trade name of polyethylene oxide produced by the Union Carbide Co.

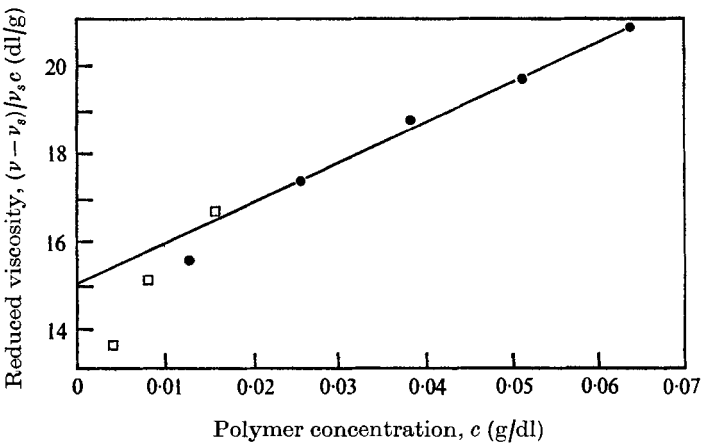

FIGURE 4. Viscometric data for WSR-301 solutions. From this graph the intrinisic viscosity and Huggins constant were found to be 15 dl/g and 0·4 respectively. $T = 25$ °C. ●, solutions prepared for intrinsic-viscosity analysis; ○, solutions used in porous-media tests.

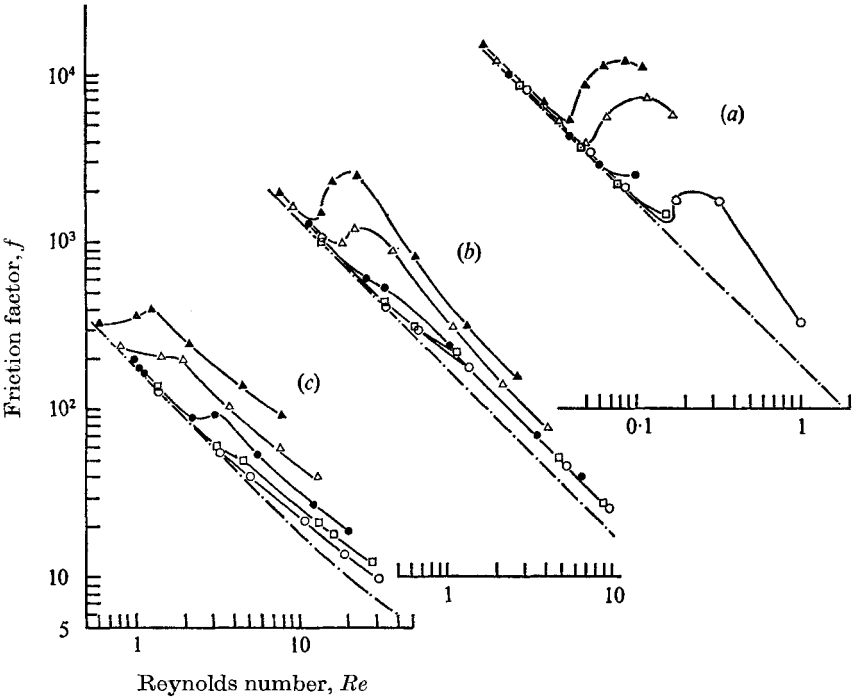

FIGURE 5. Friction-factor data for Polyox WSR-205 solutions. (*a*) 0·011 cm beads, (*b*) 0·022 cm beads, (*c*) 0·045 cm beads. —·—, Newtonian data.

	○	□	●	△	▲
Concentration (p.p.m.)	30	60	120	240	480

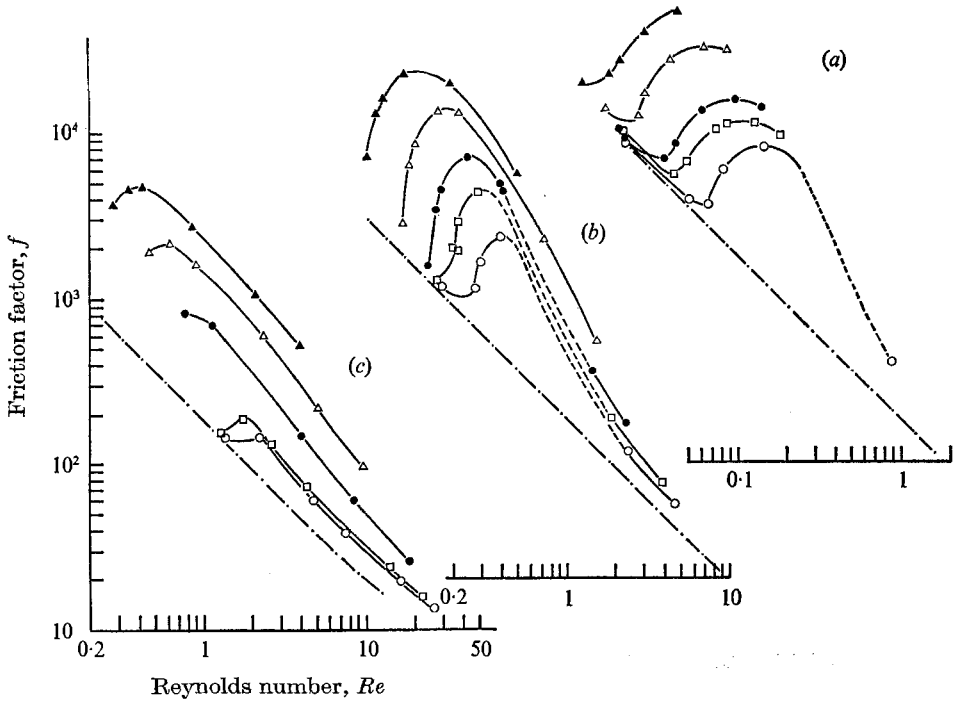

FIGURE 6. Friction-factor data for Polyox WSR-301 solutions. (*a*) 0·011 cm beads, (*b*) 0·022 cm beads, (*c*) 0·045 cm beads. —·—, Newtonian data.

	○	□	●	△	▲
Concentration (p.p.m.)	10	20	40	80	160

relationship between the reduced viscosity $(\nu-\nu_s)/\nu_s c$ and the concentration c, where ν and ν_s are the solution and solvent viscosities respectively. $[\eta]$ and Huggins' constant K were found from the equation of the straight line drawn through the data, i.e. from $(\nu-\nu_s)/\nu_s c = [\eta]+K[\eta]^2 c$; for the WSR-301 data in figure 4, these values were 15 dl/g and 0·40. Similar graphs for WSR-205 and FRA yielded the results listed in table 1; the FRA value of 0·0 for K is far removed from the usual values of 0·3–0·4, but is consistent with previous measurements made in our laboratory for this grade of Polyox.

Measurements of the flow rate and pressure drop in the three porous media were recorded for all the solutions listed in table 1. Unlike the Newtonian case, the pressure drop between adjacent pairs of taps was not always constant but usually decreased in the flow direction. This behaviour was apparently due to polymer degradation – the scission of molecular bonds by high straining – and viscometric tests of the effluent confirmed a corresponding decrease in the molecular weight. Similar behaviour has sometimes been attributed to plugging and adsorption of polymeric material on solid surfaces, though generally not for the pore sizes and concentration range encountered in the present experiments (see, for example, Sadowski, 1965; Mungan, Smith & Thompson 1966). Since the decrease in pressure drop depended on the velocity in our case and since subse-

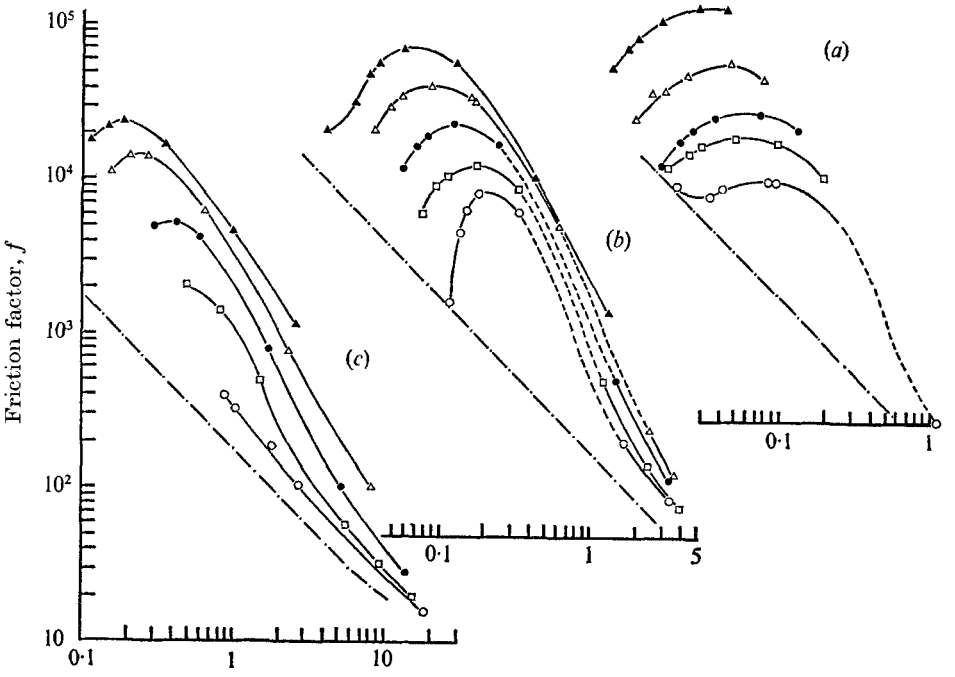

FIGURE 7. Friction-factor data for Polyox FRA solutions. (*a*) 0·011 cm beads, (*b*) 0·022 cm beads, (*c*) 0·045 cm beads. —·—, Newtonian data.

	○	□	●	△	▲
Concentration (p.p.m.)	6	12	24	48	95

quent runs with water indicated no increase in permeability, it appears that the anomaly was in fact due to degradation. The amount of degradation, judging by the change in pressure drop between the first and last pairs of taps, depended on the concentration, flow rate and bead size. For the majority of conditions the decrease in pressure drop was 10 % or less, but for some cases, particularly for the largest beads, the viscoelastic effect was substantially reduced and sometimes barely perceptible. A more detailed study of degradation appears in a subsequent section of this paper.

When degradation occurred, the average molecular weight of the polymer was lowered. In order to present results which correspond as closely as possible to the solution properties in table 1, the friction-factor data are based on the pressure drop between the first two taps, i.e. the two closest to the inlet. The results so obtained are plotted in figures 5–7, where the Ergun co-ordinates are again employed for ease of comparison with equivalent Newtonian fluids.

3. Discussion of results

Figures 5–7 show that the data at sufficiently low Reynolds numbers lie on the Newtonian line, thereby confirming that the polymer solutions behave like Newtonian fluids in this regime. This is an expected result since the deformation rates are low under these conditions and consequently the induced elasticity is too small to affect the viscosity-dominated flow. At larger Reynolds numbers, the polymer data are highly non-Newtonian; indeed, figure 7 shows that the friction factor is up to 40 times higher than the Newtonian value, an effect which is due purely to fluid elasticity since any contribution from increased viscosity is already accounted for in the Reynolds number (it should be remembered that the viscosity in Re is that of the solution and not the solvent). The data suggest that even larger pressure drops are possible with higher concentrations and such information would be desirable for practical applications. However, the present investigation was limited to dilute solutions and hence did not explore the conditions for maximum flow resistance. The extent to which the present data diverge from Newtonian values is comparable to that reported by previous investigators. Dauben & Menzie (1967), for example, also used Polyox solutions and found friction ratios as high as 35; their experimental conditions, however, were different since their beads and velocities were smaller and their solutions much more concentrated, the viscosity ranging from 1·6 to 100 cP. Similarly, Marshall & Metzner (1967) reported ratios as high as 80 using moderately concentrated solutions of polyacrylamide and beads comparable in size to our smallest.

Some of the curves drawn through the data in figures 6 and 7 contain segments which are dashed; these designate regions in which steady-state measurements of pressure and flow rate could not be obtained. This unexpected feature of the flow deserves separate attention and is therefore discussed later, in § 7.

4. Degradation

Of all drag-reducing polymers, Polyox is probably the most susceptible to degradation, and some insight into its nature was possible in the present work because the pressure drop was monitored in steps along the test section. From such measurements, it was possible to find or estimate the pressure drop for a stably degraded solution, i.e., a solution which, for a given set of flow conditions, had reached the full extent of its degradation and would degrade no further. In most cases, the pressure drop did not change after the first interval or two, and consequently the flow data for the stably degraded solutions were readily found from the last two intervals. In cases where the drop had not reached a constant value even by the last section, it was assumed that the deterioration of the solution was exponential, and the asymptotic value for the pressure drop was estimated by plotting the four available Δp's on semi-logarithmic graph paper. In this way, data for all solutions in the stably degraded state were obtained, and by comparing these values with those from the first interval, where the solutions were in the 'fresh' or minimally degraded state, it was possible to analyse the results for the causes and effects of degradation.

The most interesting characteristic which emerged was that degradation increased as the bead size increased. With the 0·045 cm beads, the molecular scission was sometimes so extensive that by the end of the test section the results were almost the same as with water, especially for the first three concentrations of each grade at the lower velocities. In contrast to this near 100 % deterioration, the same fluid at the same velocity usually suffered about 30 % degradation in the 0·022 cm bead matrix and less than 5 % with the 0·011 cm beads.

A further examination of the two sets of data revealed that, when degradation began at mid-range flow rates, the onset velocity was virtually independent of the polymer concentration. Moreover, it was found that, for various solutions of a given grade in a particular matrix, the degree of degradation was not influenced significantly by the concentration. These findings agree with the generally-held idea that the breaking of a molecular bond depends on the flow field and not on the number of molecules present (provided, of course, that they are not entangled). It is expected, therefore, that the onset and degree of degradation are functions of the strain rate, which is proportional to V/D, where $V = G/\rho$. The data show that degradation generally increased with velocity (as shown in figure 13, for example), which is physically reasonable, but the results reported in the preceding paragraph establish that degradation also increased with bead diameter. Hence V/D cannot be the controlling parameter. In essence, then, our observations support the idea that degradation increases with velocity and is independent of the concentration, but we cannot explain the apprently antithetical finding that degradation increases with the bead size.

5. Flow visualization

The large flow resistance of the dilute polymer solutions was obviously due to 'viscoelastic effects', but this phrase does not readily explain the basic mechanism. An understanding of this effect is all the more necessary when it is realized that the loss in energy must be due to viscous dissipation, and that the dissipation for polymer solutions is up to forty times higher than that for water while the steady-shear viscosity is, at most, only 30 % greater. One way of explaining this is to speculate that the flow pattern must be different, radically different in fact, in order for so much energy to be consumed. Since viscoelastic fluids often generate secondary flows (the vortex ring upstream of an orifice, for example), it was thought that the large resistance might be caused by considerable vortex motion within the cavities of the porous medium. To find out for certain, a flow-visualization study was undertaken.

Initially, an attempt was made to visualize the flow in the circular test cells, by looking at the flow next to the tube wall, but this proved more frustrating than fruitful because of problems with frontal lighting. In order to allow back-lighting and to provide a simpler flow field, a rectangular test cell was constructed, designed to contain two layers of the largest (0·045 cm) beads. The new test cell had a cross-section 5·0 × 0·075 cm and had open manometers located at the entrance and exit to determine the pressure drop along the 7·5 cm length. The streamlines were made visible by suspending 30 μm mica particles in the fluid,

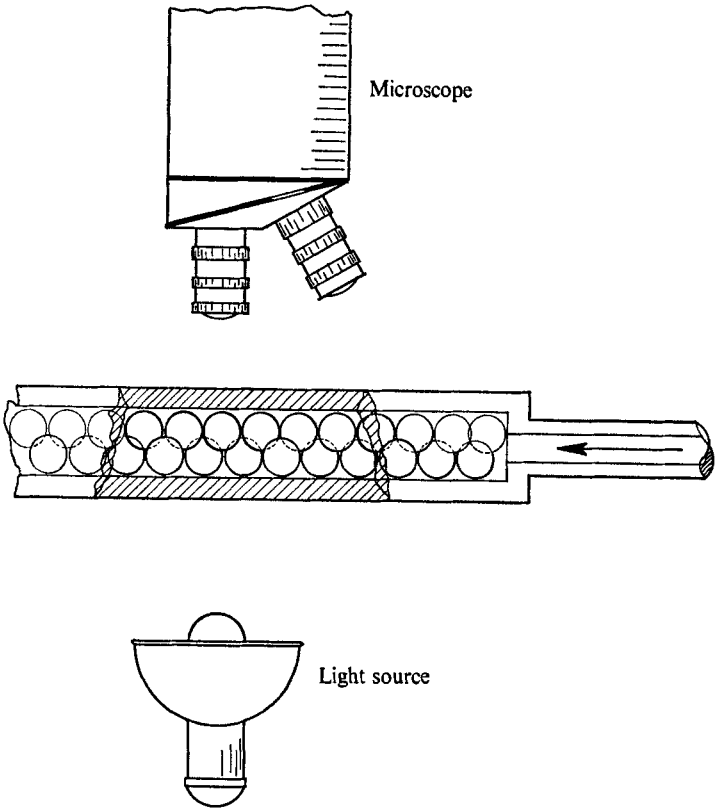

FIGURE 8. Flow visualization. The porous medium for this study consisted of two layers of beads sandwiched between lucite sheets, and the flow within the cavities was viewed with the aid of a microscope.

and were viewed through a microscope. A sketch showing the arrangement of the experimental equipment is provided in figure 8. A 100 p.p.m. FRA solution was tested at Reynolds numbers of 0·3 and 1·0, and the corresponding pressure drops were found to be 3 and 10 times that for water. The flow within the cavities was closely examined for water and the polymer solution, and for both fluids at both flow rates, the paths traced out by the illuminated mica flakes were the same.

The simple conclusion is that Newtonian fluids and dilute polymer solutions have similar streamline patterns when flowing through a porous medium. The explanation for the increased energy dissipation does not lie therefore in any changes in the flow pattern but rather in changes in the stress field due to differences in fluid rheology. Polymer solutions are known to produce normal stresses at high rates of deformation, and this nonlinear rheology must somehow be related to the observed anomalies in the pressure drop. In an attempt to understand this relationship, the deformation field and the corresponding non-Newtonian stresses are examined in the next section.

6. Non-Newtonian mechanics

In this section we shall attempt to analyse in a qualitative way how induced non-Newtonian stresses might change the pressure drop, and to examine the onset of non-Newtonian behaviour. From the combination of these studies, the mechanisms responsible for the observed effects become clearer.

6.1. *Deformation and stresses*

The first step in the analysis of the deformation field and the consequent induced stresses is an examination of the geometry of the flow passages. Since the media in the present experiments were tightly packed random arrangements of nearly uniform beads, the flow channels were quite irregular. In order to simplify the geometry without affecting the essential character of the medium, a more orderly arrangement will be studied: namely, closest packing of uniform spheres. The void fraction for this matrix is 0·26, compared with 0·37 for the test section (§ 2), which means that any values introduced in the following paragraphs might be affected, but since the values are basically in terms of orders of magnitude, no real adjustment is required. A single layer of closest packed beads is shown in figure 9(*a*), while in figure 9(*b*) there are two layers with the underneath one darkened for visual contrast. From figure 9(*a*) it is apparent that the openings for the fluid are all tricuspid in shape and figure 9(*b*) shows that these openings lead to two distinct types of flow channels, equal in number. In the case of the first, designated type *A*, the fluid passes through the tricuspid opening, impinges on a sphere in the next layer and then flows out through three equally spaced openings. A two-dimensional schematic drawing of the flow in this cavity is given in figure 9(*c*), which is an elevation view if figure 9(*b*) is the plan view. For flow through the other type of passage, denoted by *B*, the fluid enters a spacious cavity and then leaves through a tricuspid opening in the bottom. As shown in the corresponding two-dimensional schematic drawing, figure 9(*d*), there are side ports for entry and exit as well, but little flow will pass through these for a pressure gradient perpendicular to the layers of beads. (If the pressure gradient is oblique – in the flow-visualization test section, for example, it is perpendicular – the flow directions may differ from those in figure 9; but the cavity geometry is unchanged, and thus the basic motions considered here are the same.) In a type *A* cavity, the cross-sectional area of the flow does not vary significantly along the channels and consequently the deformation in these cavities is essentially shearing. In type *B*, however, the large interior means that extension and compression are also components of the deformation, in addition to shearing. Since the type *B* cavities offer much less resistance they carry most of the flow and are, therefore, the more important in determining the pressure losses through the medium. Accordingly, the subsequent analysis will deal only with these cavities.

We now examine the non-Newtonian stresses generated by each component of the deformation, that is, by shear and by pure strain, and find their separate effects on the pressure drop. It is readily acknowledged that the correct stress field cannot be found by such a decomposition, but the answers obtained do

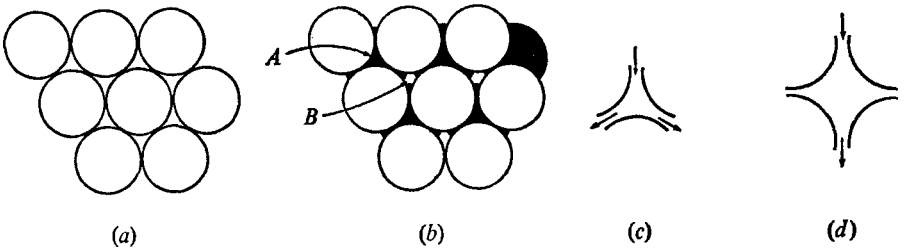

FIGURE 9. Some geometrical aspects of closest packed beads. (*a*) A single layer of beads; the fluid faces an array of tricuspid openings. (*b*) With a second layer positioned underneath (darkened for pictorial purposes), two distinct types of cavities are evident, designated *A* and *B*. (*c*) A schematic drawing of a type *A* cavity. (*d*) A schematic drawing of a type *B* acvity.

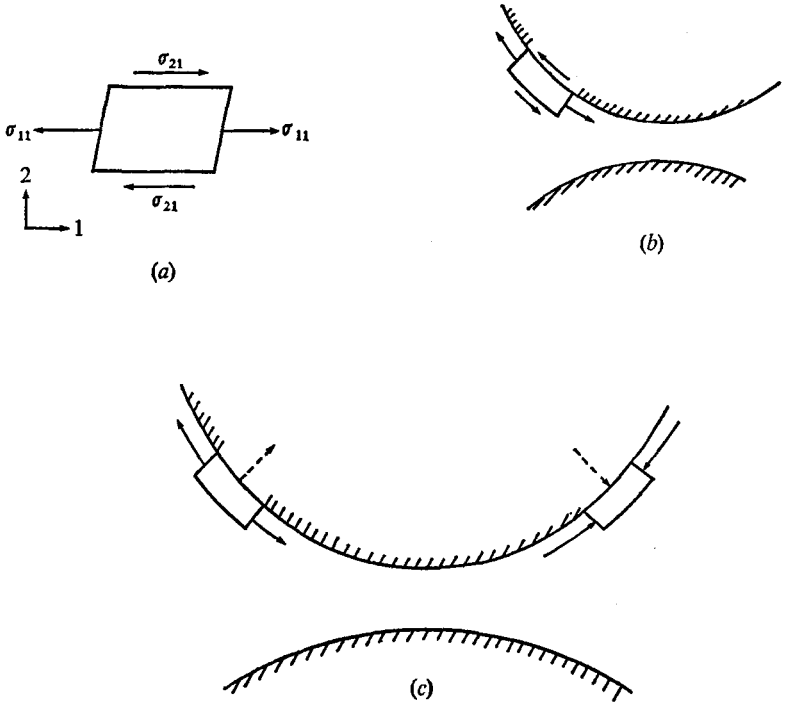

FIGURE 10. Normal stresses in shear. (*a*) For simple shearing in the 1 direction, i.e. $U_1 \propto x_2$, a normal stress σ_{11} is produced in the shearing direction. (*b*) When a fluid element is sheared on a curved surface, the normal stress acts as a hoop stress. (*c*) The normal stresses shown here are those components due only to the unsteadiness of the shear. The dashed arrows indicate the consequent stresses exerted on the wall.

appear useful in shedding some light on the fundamental mechanics of the problem. Simple shearing is considered first.

For a Newtonian fluid the only stresses are tangential, but for a polymer solution, a normal stress is induced in the shearing direction as well, as shown in figure 10(*a*). Normal stresses are induced on the other faces too, but these are generally smaller and for dilute solutions are negligible for shear rates up to $10^4\,\mathrm{s}^{-1}$. For steady shear, the ratio of the normal stress to the shear stress is $\gamma\tau$,

where γ is the shear rate and τ the fluid relaxation time, and this formula is valid for γ up to $O(\tau^{-1})$. At higher shear rates, the ratio falls off, and so the normal stress is a maximum of 10 times the shear stress. The effect of the normal stress on the pressure drop is found by studying flow through a two-dimensional convergent–divergent channel, for the force exerted on the walls will be a measure of the drag force on spheres in a three-dimensional flow. On a curved surface, the normal stress acts as a hoop stress as shown in figure 10(*b*). When the channel is symmetrical, the shear rate is the same at points equidistant upstream and downstream from the midpoint (throat), so that there is no net force exerted on the walls. However, when the shear is unsteady, as it is in an expansion or contraction, the normal stress is augmented above its steady-shear value when the shear rate is increasing and diminished when it is decreasing. The amount of augmentation is small, as shown by the molecular model or from constitutive equations based on the model, for the maximum amplification factor is 2 for the extreme case of a step increase in shear. This component of the stress, viz., that due to unsteadiness alone, is shown in figure 10(*c*): the arrows indicate that it is positive on the upstream side and negative on the downstream side, so that the net effect is to increase the drag on the surface (and, therefore, increase the pressure drop). The extent of the increase may be estimated by assuming any reasonable velocity profile extending outwards from the surface, and by doing so it was found that the non-Newtonian effect has the same order of magnitude as the Newtonian component. Consequently the increase in pressure loss due to shear effects only is $O(1)$.

In a similar way, the effect of pure straining may be examined. By pure straining is meant deformation in which there is no rotation and no shear, so that, if the flow is again simplified to two dimensions, the streamlines are necessarily hyperbolas.† During this type of deformation, rectangular elements remain rectangular as shown in figure 11(*a*). The stresses indicated on the element surfaces are the components due to the elastic or non-Newtonian character of the fluid, viz., these stresses are over and above those accounted for by viscosity. The component in the streamwise direction may be very large; in fact, the Rouse–Zimm molecular model or constitutive relations of the Maxwell type predict that this particular stress behaves like $(1-2\gamma\tau)^{-1}$. The actual stress does not become unbounded as the shear rate approaches $(2\tau)^{-1}$ of course, but experiments have shown that its magnitudes are indeed large (Metzner & Metzner 1970). To determine the effect of these stresses, the convergent–divergent channel is assumed to have a form such that the deformation of the fluid within is always pure strain. This means that the channel walls are segments of hyperbolas, as shown in figure 11(*b*), and that the fluid is imagined to slip along these surfaces, say over a very thin boundary layer. In this case, it is convenient to consider triangular fluid elements, with the oblique face tangential to the wall. For the element shown on the upstream side in figure 11(*b*), the stresses on the perpendicular faces are those for pure extension as depicted in figure 11(*a*). In the absence of inertial

† In order that the vorticity $\partial u/\partial y - \partial v/\partial x$ and the shear rate $\partial u/\partial y + \partial v/\partial x$ be zero, $u = u(x)$ and $v = v(y)$. Furthermore, to satisfy continuity, $u = ax$ and $v = -ay$ (a = constant), in which case the streamlines are hyperbolas.

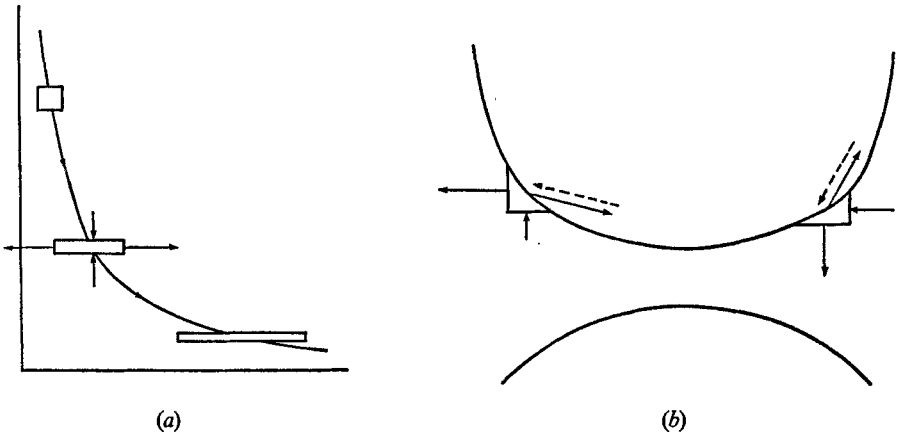

(*a*) (*b*)

FIGURE 11. Normal stress in pure strain. (*a*) The deformation of a rectangular element during pure strain. The arrows indicate non-Newtonian stresses, i.e. stresses over and above those due to viscosity alone. (*b*) The balance of stresses on a triangular element, adjacent to the wall, in a channel designed such that the fluid first undergoes pure extension and then pure compression. As in the previous figure, the dashed arrows represent the stresses exerted by the fluid on the wall.

effects, the stress on the oblique face must balance the other two, and consequently the stress exerted by the fluid on the wall is in the direction indicated by the dashed arrow. The same type of reasoning can be applied to an element, on the upstream wall, undergoing pure compression. In this case, the directions of the normal stresses are reversed and the stress exerted on the wall is again shown by a dashed arrow. The direction of the dashed arrows demonstrates that the effect of pure straining is to produce a drag force whose direction is opposite to the streaming direction, which is equivalent to reducing the pressure drop. This startling result appears contrary to intuition, but the physics do make sense when it is remembered that the flow was idealized to suppress the effects of shear. The context for this particular finding will become apparent and easier to discuss once the onset of non-Newtonian behaviour has been examined.

6.2. *Onset*

The onset of non-Newtonian behaviour in figures 5–7 may easily be identified in many instances. Some general conclusions about onset were found from the data, and then these results were combined with an analysis of flow past closest packed spheres to yield estimates of the fluid deformation rate at onset.

From figures 5–7, the onset Reynolds number Re_0 was found or approximated for over half the cases, and these values were used to compute the onset velocity $V_0 \equiv (1-\epsilon)\nu Re_0/D$. The quantity V was introduced earlier and is equal to G/ρ or to Q/A, where Q is the flow rate and A the total cross-sectional area of the flow. V is sometimes termed the superficial velocity, but is a poor measure of fluid speeds in the matrix since it is equivalent to the mean velocity if there were no beads present. The ratio V/D therefore underestimates the strain rate but is directly related to it. This relationship will be found in subsequent paragraphs,

WSR-205 conc. (p.p.m.)	Bead size (cm) 0·011	0·022	0·045	WSR-301 conc. (p.p.m.)	Bead size (cm) 0·011	0·022	0·045	FRA (p.p.m.)	Bead size (cm) 0·011	0·022
30	7·7	5·5	12·1	10	3·3	3·0	3·9	6	1·2	1·7
60	6·4	5·5	9·9	20	2·1	2·0	3·9	12	0·9	0·9
120	4·2	3·8	6·8	40	1·7	1·8	—	24	1·0	—
240	3·3	3·0	2·9	80	1·2	1·2	—	48	0·55	—
480	3·1	2·6	2·2	160	0·7	0·9	—	96	0·41	0·20

TABLE 2. The onset of non-Newtonian behaviour. Values of V_0/D (s^{-1})

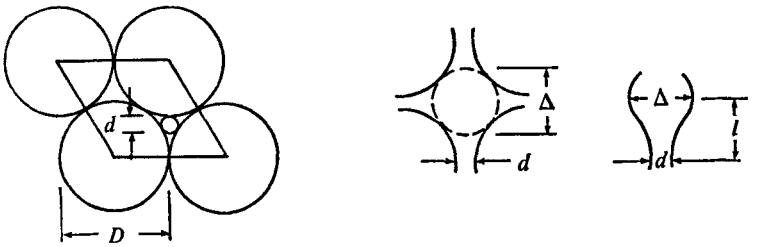

(*a*) (*b*) (*c*)

FIGURE 12. (*a*) The flow through a tricuspid opening is considered comparable to flow through a tube which just fits the opening and carries nearly the same flow rate. The tube diameter d is (cosec $30° - 1$) D. (*b*) A schematic drawing to show the largest sphere which just fits a type B cavity; the sphere diameter Δ is found to be $(\sqrt{2} - 1)\,D$. (*c*) The flow through a type B cavity is assumed to be comparable to flow through a circular non-uniform channel having the dimensions shown.

but meanwhile it is useful to examine the available onset values V_0/D for they are readily found from the experimental data and provide qualitative information. These data are given in table 2 and show that V_0/D is roughly constant for a given fluid; that is, the variation in V_0/D is no larger than the error in estimating Re_0 from the graphs, and is much smaller than the fourfold variation in D. These data, therefore, verify the expectation that onset occurs when the strain rate is sufficiently large. The results also indicate that, for a series of solutions of a particular grade and a particular bead size, the onset shear rate decreases as the concentration increases. It might be thought that V_0/D should be constant, or nearly so, since the present solutions were reasonably dilute. Yet of the great variety of experiments conducted with Polyox solutions, very few have shown concentration-independent onset behaviour in the dilute regime. This variation is probably due to the broad distribution of molecular weights in commercial Polyox samples.

In attempting to establish reliable values for the actual strain rates, it is first noted that the deformation rate varies considerably throughout the flow channels and generally consists of both shear and pure strain. Accordingly, our efforts here are directed to finding the maximum amplitude of each component at a given flow rate. Again, attention is focused on the type B cavities and, as before, shear is considered first. This component is largest where the cross-section of the flow

is smallest, namely in the tricuspid opening described earlier and shown again in figure 12 (*a*). The maximum rate of shearing occurs at the wall and is estimated by finding the equivalent wall shear rate in a tube which just fits the opening and which carries most of the flow passing through this opening, say 90 %. Since little flow passes through type *A* cavities, the flow carried by the tubes is about three-quarters of the total, the fraction hereafter denoted by k. The mean velocity V_m in the tube is related to the superficial velocity V by the ratio of the tube area $\frac{1}{4}\pi d^2$ to the area of the diamond shown in figure 12 (*a*) (the diamond is the smallest subdivision of the entire cross-sectional area which contains two tricuspid openings); since the area of the diamond is $\frac{1}{2}D^2\sqrt{3}$, by continuity

$$V_m = \frac{k2\sqrt{3}}{\pi}\left(\frac{D}{d}\right)^2 V.$$

The shear rate at the tube wall is $8V_m/d$, which is assumed to be equivalent to the maximum rate of shear γ_{sh} in the porous medium; accordingly, after substituting $d = (\mathrm{cosec}\,30° - 1)\,D$,

$$\gamma_{sh} = \frac{k16\sqrt{3}}{\pi(\mathrm{cosec}\,30° - 1)^2}\left(\frac{V}{D}\right) \simeq 1800\left(\frac{V}{D}\right).$$

Since the onset values of V/D in table 2 are $O(1)\,\mathrm{s}^{-1}$, the onset values for the shear rate are estimated to be $O(10^3)\,\mathrm{s}^{-1}$.

When finding the corresponding values for the pure-strain component of the deformation, the problem becomes one of estimating the rate of extension (or compression) for flow through a type *B* cavity. Again the irregular geometry is simplified, in this case by assuming that the most characteristic dimension of the interior is the diameter Δ of a sphere which just fills the cavity, as shown schematically in figure 12 (*b*). The straining of fluid in the cavity is, therefore, considered to be comparable to that for an axisymmetric channel of maximum diameter Δ and minimum diameter d, as illustrated in figure 12 (*c*). As before, it is presumed that a fraction k of the total flow rate passes through the channel, and because of the low Reynolds numbers throughout, a parabolic velocity profile is assumed at the maximal and minimal cross-sections. The maximum rate of (pure) strain γ_{st} occurs along the centre-line and is, therefore, estimated by finding the difference in centre-line velocity over the distance l, and dividing by l. Since the centre-line velocity is twice the mean and since the latter was found for the minimum cross-section in the preceding paragraph,

$$\gamma_{st} = \frac{k4\sqrt{3}}{\pi l}\left[\left(\frac{D}{d}\right)^2 - \left(\frac{D}{\Delta}\right)^2\right] V.$$

For closest packing of spheres, it is straightforward to show that $\Delta = (\sqrt{2} - 1)\,D$ and $l = D/\sqrt{6}$, so that

$$\gamma_{st} = \frac{k12\sqrt{2}}{\pi}\left[(\mathrm{cosec}\,30° - 1)^{-2} - (\sqrt{2} - 1)^{-2}\right]\left(\frac{V}{D}\right) \simeq 150\left(\frac{V}{D}\right).$$

Since V_0/D is $O(1)\,\mathrm{s}^{-1}$, the maximum rate of extension or compression at onset is $O(10^2)\,\mathrm{s}^{-1}$.

These estimates of the deformation rates in shear and pure strain become more meaningful when considered along with the characteristic time for a fluid, namely the largest Rouse relaxation time τ_1. These times, computed from

$$\tau_1 = 6\eta_s[\eta]M/\pi^2RT$$

(Rouse 1953), are 0·00010, 0·0014 and 0·0060 s for our WSR-205, WSR-301 and FRA grades. Using these times with the preceding formulae for γ_{sh} and γ_{st}, and with the onset data in table 2, it is found that the dimensionless shear rate $\gamma_{sh}\tau_1$ at onset is $O(10)$ and the dimensionless pure strain rate $\gamma_{sh}\tau_1$ is $O(1)$. The discussion in § 6.1 indicated that these are just the orders of magnitude when each component can be expected to produce departure from Newtonian behaviour. The departure, however, is more probably due to extension than shear. As analysed earlier, non-Newtonian shear cannot affect the pressure drop by more than $O(1)$, whereas the effects due to extension may be much larger, and hence more compatible with the observed effects, because of the $(1-2\gamma_{st}\tau_1)^{-1}$ behaviour. It is not yet clear, though, just how the extensional stresses act to increase the drag force on the beads. From the results of our analyses in § 6.1, it now becomes apparent that the shear and pure strain must be coupled such that the extensional stresses produce large tangential stresses on the solid surfaces. Also, it is not quite clear what mechanism is responsible for the decline in non-Newtonian deviation at higher flow rates. A partial answer is suggested, of course, by the analysis in § 6.1 of the effects of pure strain: it may be that, at the higher deformation rates, the normal stresses produced by pure strain become more and more dominant in the stress field and bring about the result predicted in § 6.1, namely a reduction of the drag force. These ideas are of course no more than conjecture; yet until a more complete analysis is available, they provide a plausible means of explaining the observed results, consistent with the known mechanics of dilute polymer solutions.

7. A velocity gap

As mentioned earlier, the dashed curves in figures 6 and 7 denote regions in which it was impossible to achieve a steady flow. This aspect of the work was not fully explored, but the present data are sufficient to establish the essential characteristics. The phenomenon can be understood most readily when the flow data are plotted in dimensional co-ordinates, rather than as dimensionless groups as in figures 6 and 7. As an illustration, the results for three FRA solutions are plotted in this way in figure 13. The figure contains points for stably degraded as well as fresh solutions, partly to provide some degradation data and partly to demonstrate that the phenomenon can occur with both types of solution. The characteristic behaviour can be seen from the figure: a sharp rise in pressure with velocity at low flow rates, a maximum viscoelastic effect and a fairly quick return to near-Newtonian values at higher flow rates; that is, the non-Newtonian behaviour occurs over a relatively narrow range of flow rates. For all three solutions in figure 13, the flow rate rose slowly as the driving pressure was increased, up to a velocity of 0·08 cm/s. For the 96 p.p.m. solution, the flow rate increased continuously as the pressure rose still further. For the other two solu-

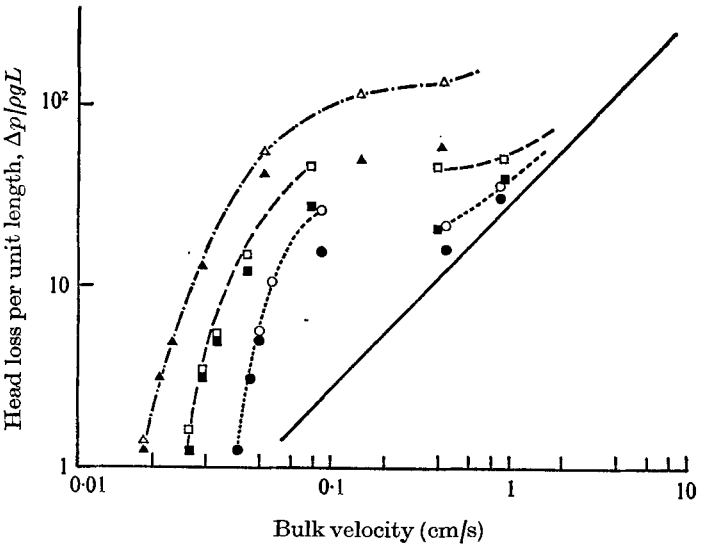

FIGURE 13. Pressure-drop measurements for fresh (open symbols) and stably degraded solutions (solid symbols) of FRA in the 0·022 cm bead matrix. The gaps in the 6 and 24 p.p.m. curves indicate regions in which steady-state measurements could not be obtained. ——,water. FRA: ----○----, 6 p.p.m.; ——□——, 24 p.p.m.; —·—△—·—, 96 p.p.m.

tions, however, the velocity jumped to around 0·4 cm/s and it was found that the flow would stabilize at the higher flow rate at a pressure below that prior to the jump; when the pressure was further increased, the velocity correspondingly rose above 0·4 cm/s. In the region between 0·08 and 0·4 cm/s, it was impossible to attain steady-state measurements, which is readily understandable from the graph since the pressure–flow curve has a negative slope there and the situation is inherently unstable. The curve has not been drawn in this region in figure 13 and is represented by the dashed segments in figures 6 and 7. It should be noted here that the same results were obtained when the run started at the maximum pressure and flow rate and data were recorded as the pressure was reduced. The phenomenon arises from the fact that the pressure drop for these nonlinear fluids does not necessarily increase monotonically with the flow rate, but apparently can be a multi-valued function under some conditions. Hence when the flow is driven by a constant head, there is a range of velocities in which steady-state measurements cannot be made, and a 'velocity gap' appears in the pressure–flow curve.

Similar graphs for other solutions confirmed that the velocity gap appeared only when the viscoelastic effect was pronounced and confined to a small velocity range, small enough, at least, to produce a negative slope in the pressure–flow curve. The WSR-205 solutions deviated from Newtonian behaviour only moderately and thus their data were always continuous. For flows of the other two grades past the 0·045 cm beads, the viscoelastic effect was invariably large (as figures 6 and 7 show) but it remained large even at high velocities and consequently the data for these flows were continuous as well. These two figures also indicate that, for the 0·011 cm beads, the velocity gap occurred only for the lowest

concentration of WSR-301 and FRA. However, when the data for all concentrations were plotted in dimensional form (like figure 13 but not shown here), it was apparent that solutions of higher concentration would also have exhibited this effect if the driving pressure had been increased sufficiently.

Figure 13 suggests that this phenomenon might be caused by degradation, since it occurs when the degree of degradation becomes significant. Yet the data for the stably degraded solutions (the solid symbols) have negative slope too, indicating that the gap may appear for undegradable, as well as degradable, solutions. Consequently, while degradation and the discontinuity may both be a result of high flow rates, the two effects do not appear to be related.

This velocity gap is a new and interesting aspect of the flow of dilute solutions through porous media. It is not a general phenomenon, and occurs only when the viscoelasticity induced by the flow is pronounced and limited to a short velocity range, conditions which are met by dilute high-weight Polyox solutions in media with a pore size $O(10^{-2})$ cm.

The authors acknowledge with gratitude the support of this work by the National Research Council of Canada, and the assistance of Don Murray in reducing the data and visualizing the flow.

REFERENCES

BIRD, R. B., STEWART, W. E. & LIGHTFOOT, E. N. 1964 *Transport Phenomena*, 4th corrected printing. Wiley.

CHRISTOPHER, R. H. & MIDDLEMAN, S. 1965 *Indust. Engng Chem. Fund.* **4**, 422–426.

DAUBEN, D. L. & MENZIE, D. E. 1967 *J. Petrol. Tech.* **19**, 1065–1072.

ERGUN, S. 1952 *Chem. Enging Prog.* **48**, 89–94.

JAMES, D. F. & ACOSTA, A. J. 1970 *J. Fluid Mech.* **42**, 269–288.

JONES, W. M. & MADDOCK, J. L. 1969 *Brit. J. Appl. Phys., J. Phys.* D **2** (2), 797–808.

MARSHALL, R. J. & METZNER, A. B. 1967 *Indust. Engng Chem. Fund.* **6**, 393–400.

METZNER, A. B. & METZNER, A. P. 1970 *Rheol. Acta*, **9**, 174–181.

MUNGAN, N., SMITH, F. W. & THOMPSON, J. L. 1966 *Trans. Soc. Petrol. Engng*, **237**, 1143–1150.

ROUSE, P. E. 1953 *J. Chem. Phys.* **21**, 1272–1283.

SADOWSKI, T. J. 1965 *Trans. Soc. Rheol.* **9**, 251–271.

SAVINS, J. G. 1969 *Indust. Engng Chem.* **61**, 18–47.

SHIN, H. 1965 Sc. D. thesis, Massachusetts Institute of Technology.